Journal of Power Sources 192 (2009) 132–137

Contents lists available at ScienceDirect

Journal of Power Sources

journal homepage: www.elsevier.com/locate/jpowsour

$SrCo_{1-x}Sb_xO_{3-\delta}$ perovskite oxides as cathode materials in solid oxide fuel cells

A. Aguadero[a,*], D. Pérez-Coll[a], C. de la Calle[b], J.A. Alonso[b], M.J. Escudero[a], L. Daza[a,c]

[a] Centro de Investigaciones Energéticas Medioambientales y Tecnológicas (CIEMAT), Av. Complutense 22, 28040 Madrid, Spain
[b] Instituto de Ciencia de Materiales de Madrid (CSIC), Cantoblanco, 28049 Madrid, Spain
[c] Instituto de Catálisis y Petroleoquímica (CSIC), C/Marie Curie 2, Campus Cantoblanco, 28049 Madrid, Spain

ARTICLE INFO

Article history:
Received 15 October 2008
Received in revised form 11 December 2008
Accepted 31 December 2008
Available online 14 January 2009

Keywords:
Electrode
Impedance spectroscopy
Solid oxide fuel cells
Strontium cobaltite
Phase stabilization

ABSTRACT

The $SrCo_{1-x}Sb_xO_{3-\delta}$ ($x = 0.05$, 0.1, 0.15 and 0.2) system was tested as possible cathode for solid oxide fuel cells (SOFCs). X-ray diffraction results show the stabilization of a tetragonal *P4/mmm* structure with Sb contents between $x = 0.05$ and $x = 0.15$. At $x = 0.2$ a phase transition takes place and the material is defined in the cubic *Pm-3m* space group. In comparison with the undoped hexagonal $SrCoO_3$ phase, the obtained compounds present high thermal stability without abrupt changes in the expansion coefficient. In addition, a great enhancement of the electrical conductivity was observed at low and intermediate temperatures ($T \leq 800\,^{\circ}C$). The sample with $x = 0.05$ displays the highest conductivity value that reaches 500 S cm^{-1} at 400 °C and is over 160 S cm^{-1} in the usual working conditions of a cathode in SOFC (650–900 °C). Moreover, the impedance spectra of the $SrCo_{1-x}Sb_xO_{3-\delta}/Ce_{0.8}Nd_{0.2}O_{2-\delta}/SrCo_{1-x}Sb_xO_{3-\delta}$ ($x \geq 0.05$) symmetrical cells reveal polarization resistances below 0.09 Ω cm^2 at 750 °C which are much smaller than that displayed by the pristine $SrCoO_{3-\delta}$ sample. The composition with $x = 0.05$ shows the lowest ASR values ranging from 0.009 to 0.23 Ω cm^2 in the 900–600 °C temperature interval with an activation energy of 0.82 eV.

1. Introduction

One of the major requirements for the commercialization of solid oxide fuel cells (SOFC) is the development of new mixed ionic-electronic conductors as cathode materials with better performance at lower temperatures (650–850 °C) that also fulfil with the cell requirements. High-temperature $SrCoO_{3-\delta}$ phases with cubic 3C-like crystal structures are mixed conductors with very high oxygen permeability values [1,2]. At room temperature and normal pressure, $SrCoO_{3-\delta}$ oxides show an approximate stoichiometry of $Sr_2Co_2O_5$ with two different polymorphs. If the samples are quenched from the reaction temperature (~1000 °C) an orthorhombic brownmillerite-type structure is obtained. In this metastable phase the oxygen vacancies are long-range ordered in layers of isolated MO_4 tetrahedral zigzag chains, alternating with octahedral layers [3]. However, if the samples are slowly cooled from the reaction temperature (~1000 °C), a hexagonal polymorph is obtained, with a structure related to that of 2H-$BaNiO_3$ [4]. Further studies have demonstrated that the crystal structure of the hexagonal phase could be described as a face-sharing arrangement of CoO_6 octahedra [5–7] and that this polymorph is, in fact, slightly Co-deficient, acquiring the $Sr_6Co_5O_{15}$ chemical stoichiometry [8]. This hexagonal structure has shown to be almost non-oxygen permeable [1]. Moreover, at temperatures above 900 °C it undergoes a phase transition to a cubic C-perovskite with abrupt changes in the expansion coefficient that could produce cracking problems during the cell operation [9].

Among the various phase structures of $SrCoO_{3-\delta}$, the oxide with the cubic symmetry shows the highest electronic and ionic conductivity values. However, the structural transition to the hexagonal phase at temperatures below 900 °C is an important handicap for high temperature electrochemical devices. The room temperature stabilization of the $SrCoO_{3-\delta}$ cubic perovskite has been achieved by doping with several elements [10–12]. However, it has also been observed that the oxygen permeability and electrical conductivity in the related solid solutions increase with decreasing the concentration of the substituting cations in Sr and Co positions [13,14].

In a previous work we have stabilized a tetragonal perovskite phase by doping the $SrCoO_{3-\delta}$ system with 10% of Sb in the cobalt position obtaining a great improvement of the electrical properties compared to the undoped hexagonal phase [15]. In this work, we aim to study the effect of the doping content along the $SrCo_{1-x}Sb_xO_{3-\delta}$ system ($x = 0.05$, 0.1, 0.15 and 0.2) and its potential as SOFC cathode material. For this purpose, the structural, mechanical, electrical and electrochemical properties have been analyzed.

2. Experimental

The synthesis of the $SrCo_{1-x}Sb_xO_{3-\delta}$ ($x = 0.05$, 0.1, 0.15 and 0.2) series was performed via the nitrate-citrate route. For this pur-

* Corresponding author.
E-mail address: ainara.aguadero@gmail.com (A. Aguadero).

0378-7753/$ – see front matter © 2009 Elsevier B.V. All rights reserved.
doi:10.1016/j.jpowsour.2008.12.138

pose, stoichiometric amounts of commercial Sb_2O_3, $Sr(NO_3)_2$ and $Co(NO_3)_2{\cdot}6H_2O$ were dissolved in a citric acid aqueous solution containing some drops of HNO_3 (65%). The solutions were slowly evaporated, leading to an organic resin which was dried at 120 °C and slowly decomposed at 600 °C. The obtained precursors were then heated at 900 °C for 12 h and at 1000 °C for 24 h with intermediate grinding. After the thermal treatments, the samples were slow-cooled in the furnace.

The freeze-drying precursor route [16,17] was used to prepare the $Ce_{0.8}Nd_{0.2}O_{2-\delta}$ (20CNO) electrolyte material. Stoichiometric amounts of the involved cations were dissolved in distilled water using $Ce(NO_3)_3{\cdot}6H_2O$ (Aldrich, 99.99%) and $Nd(NO_3)_3{\cdot}6H_2O$ (Aldrich, 99.9%) as reactants The solutions were frozen in liquid nitrogen and introduced in a freeze-dryer (Heto Lyolab) for 3 days. The amorphous powders were then calcined at 375 °C for 4 h to decompose the nitrates. Sintered pellets of about 7 mm diameter and 1 mm thickness were prepared by uniaxial pressing after milling the powders (precalcined at 375 °C) with zirconia balls and heating at 1500 °C for 10 h.

The obtained powders were characterized by X-ray diffraction in order to assess phase purity and crystallinity. The structural characterization was determined by Rietveld analysis of the X-ray data using the FULLPROF suite program.

In order to analyze the chemical compatibility of cathodes and electrolytes, XRD measurements were performed in mixtures of powders of 20CNO electrolyte and the cathode materials after being calcined at 1000 °C for 4 h and 850 °C for 50 h.

Thermogravimetric (TG) and differential thermal analysis (DTA) in air were performed using a Stanton STA 781 instrument in the range of 25–900 °C. In reducing conditions they were performed in a Mettler Toledo STAR SW 9.01 instrument, in the 30–900 °C temperature range, under a 10%H_2/90%N_2 flow (100 ml min^{-1}). About 50 mg were used in each experiment. An OmniStar™ mass spectrometer was coupled to the TG system to analyze the gases formed during the processes.

Thermal expansion coefficients and electrical conductivities of the $SrCo_{1-x}Sb_xO_{3-\delta}$ system were measured in sintered samples prepared by pressing the powders in cylindrical pellets (10 mm in diameter and about 1.4 mm in thickness) and calcining at 1200 °C for 5 h.

The electrical conductivity of the system was measured in air by the Van der Pauw DC four probe method. The measurements were carried out in the temperature range of 350–950 °C. The dense ceramics were placed on an alumina support and four platinum-wire contacts were pressed onto the surface of the pellets using a spring loaded alumina tube. A current load ranging from 0.5 to 1 A was applied by a DC power source (Agilent E3646 A) and the potential drop was recorded by a Fluke 179 True RMS Multimeter.

AC impedance spectroscopy measurements were carried out in air conditions on symmetrical cells of $SrCo_{1-x}Sb_xO_{3-\delta}$/$Ce_{0.8}Nd_{0.2}O_{2-\delta}$/$SrCo_{1-x}Sb_xO_{3-\delta}$ (*x*SCSb//20CNO). For this purpose inks of the cathode materials and a binder (Decoflux™, WB41, Zschimmer and Schwartz) were prepared and symmetrically painted onto the surfaces of the sintered pellets obtaining 5.50 mm-diameter symmetrical electrodes. The cells were calcined at 1000 °C for 4 h to obtain a good adherence between the cathodes and the electrolytes. Subsequently, two Pt electrodes were painted onto the cathode surfaces and calcined at 950 °C for 1 h to ensure equipotential conditions.

The symmetrical cells were placed into a ceramic support and four Pt wires were used to supply the current and record the voltage drop through the system. Impedance measurements were performed from 550 to 850 °C in air, using an AUTOLAB FRA system (PGSTAT30 and FRA2 module) from Eco Chemie B.V. The measurements were carried out in potentiostatic mode from 1 MHz to 10 mHz in open circuit conditions with a signal amplitude of 50 mV.

3. Results and discussion

3.1. Structural characterization and chemical compatibility

The synthesis of pure and well crystallized powders of the $SrCo_{1-x}Sb_xO_{3-\delta}$ series and $Ce_{0.8}Nd_{0.2}O_{2-\delta}$ was checked by X-ray diffraction measurements. The sample $x = 0.1$ was previously described in the tetragonal *P4/mmm* space group with $a = a_0$, $c = 2a_0$ ($a_0 \approx 3.9$ Å) by neutron powder diffraction studies [15]. In this structure, flattened and elongated $(Co,Sb)O_6$ octahedra were alternatively distributed along the *c* axis, sharing corners in a three-dimensional array (3C-like structure). The oxygen vacancies were located in the equatorial oxygen positions; these oxygens presented high thermal factors suggesting high ionic mobility. It was also observed a phase transition to a cubic perovskite unit cell, in the temperature range of 500–700 °C.

In this work, the crystal structure of the $SrCo_{1-x}Sb_xO_{3-\delta}$ compounds was determined by Rietveld refinement from X-ray diffraction data using the Fullprof Suite program. The low-Sb content oxides ($x \leq 0.15$) were adequately described with the tetragonal *P4/mmm* space group previously described (Fig. 1a). However, a cubic *Pm-3m* space group was used to describe the crystal structure of the $x = 0.2$ oxide, considering that Sb atoms are distributed at random over the Co positions, and the oxygen vacancies are also randomly distributed in the oxygen sublattice (Fig. 1b). Fig. 2 shows the variation of the unit cell parameters with the Sb content in which the tetragonal to cubic phase transition is observed for $x = 0.2$.

In order to assess the chemical compatibility between the $SrCo_{1-x}Sb_xO_{3-\delta}$ ($x = 0.05$, 0.1, 0.15 and 0.2) cathode materials and

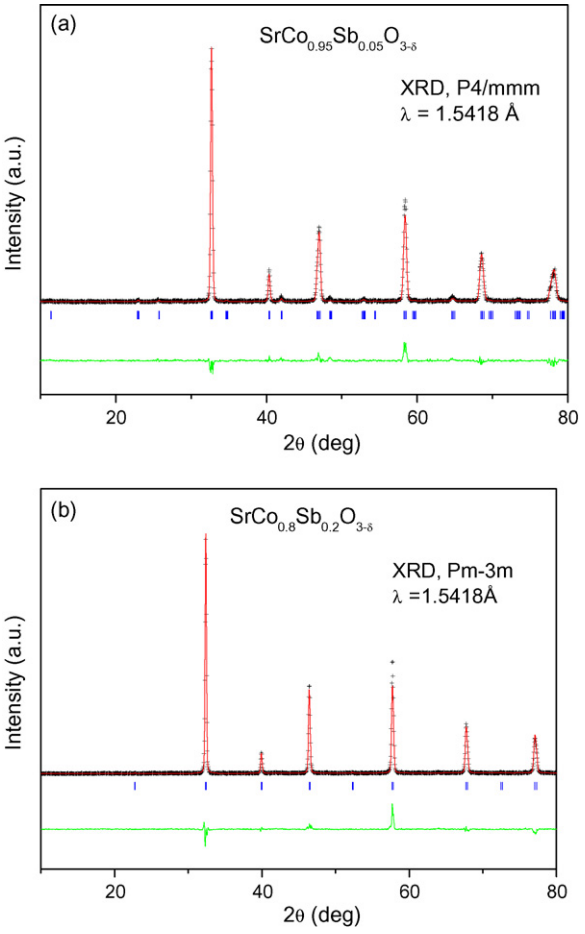

Fig. 1. Rietveld refinement from XRD data (a) in the tetragonal *P4/mmm* space group for the $x = 0.05$ sample and (b) in the cubic *Pm-3m* space group for the $x = 0.2$ sample.

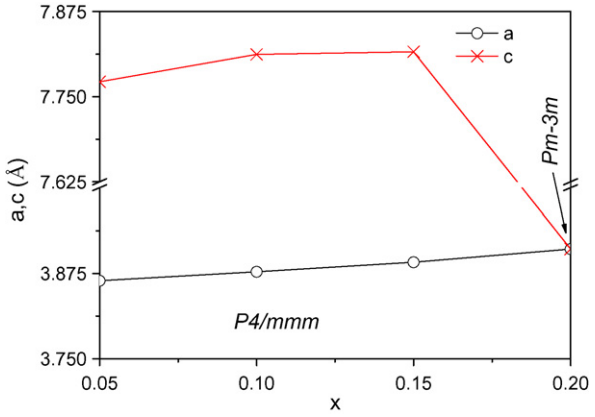

Fig. 2. Variation of the unit-cell parameters with the Sb content along the $SrCo_{1-x}Sb_xO_{3-\delta}$ series. A phase transition occurs at $x = 0.2$ from a tetragonal *P4/mmm* to a cubic *Pm-3m* structure.

the 20CNO electrolyte, mixtures of the powders in a ratio of 2:1 (w:w, cathode:electrolyte) were calcined at 1000 °C (4 h) and subsequently at 850 °C (50 h). XRD diagrams of the calcined mixtures did not reveal chemical reaction between the cathodes and the electrolyte, avoiding the formation of unwanted secondary phases as it is observed in Fig. 3 for $x = 0.1$.

3.2. Thermogravimetric and differential thermal analysis

The oxygen content of $SrCo_{1-x}Sb_xO_{3-\delta}$ ($x = 0.05$, 0.1, 0.15 and 0.2) was determined by thermogravimetric analysis under reducing conditions (10%H_2/90%N_2) from 300 to 900 °C. The oxygen release was followed by the formation of water using a mass spectrometer coupled to the TG instrument. After cooling the samples, the final products were identified by XRD as a mixture of SrO, metallic Co and Sb_2O_3. Fig. 4 evidences that, along the series, the compounds $SrCo_{1-x}Sb_xO_{3-\delta}$ display an increase in the oxygen content (decrease of the oxygen vacancies, δ) concomitant with the increment of Sb content.

In order to study the thermal stability of the $SrCo_{1-x}Sb_xO_{3-\delta}$ system, simultaneous TG and DTA measurements were performed in air between 25 and 1000 °C during heating and cooling processes. In all the studied samples the TG curves show a weight loss starting at around 400 °C and monotonously increasing up to 1000 °C, accompanied by a broad endothermic peak around 400–500 °C in

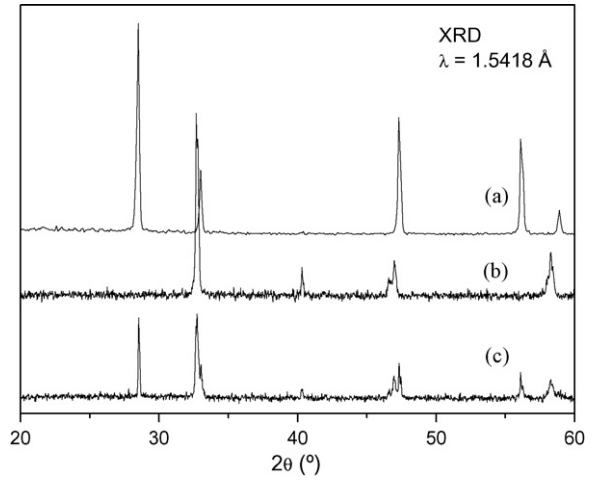

Fig. 3. XRD patterns for (a) pure 20CNO, (b) pure $SrCo_{0.9}Sb_{0.1}O_{3-\delta}$ and (c) mixture of $SrCo_{0.9}Sb_{0.1}O_{3-\delta}$ and 20CNO calcined at 1000 °C, 4 h and subsequently at 850 °C, 50 h.

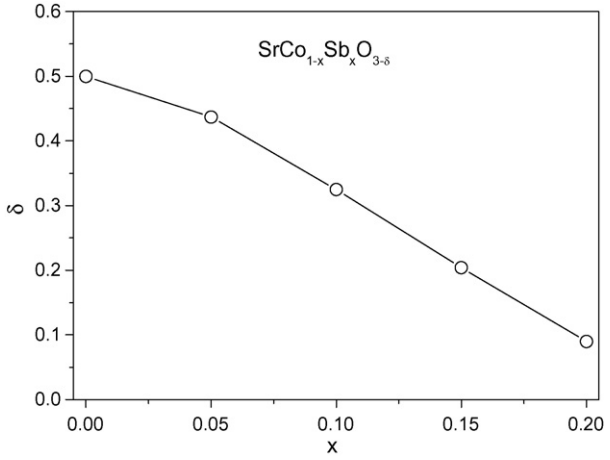

Fig. 4. Variation of the oxygen vacancies content (δ) with the Sb content in the $SrCo_{1-x}Sb_xO_{3-\delta}$ system.

the DTA curves (Fig. 5). This weight loss would probably be due to the oxygen release from the sample leading to the reduction of Co cations. It has also been observed a slight endothermic peak at around 900 °C for all the compositions under study. However, in our previous work [15], no structural transitions where found for $SrCo_{0.9}Sb_{0.1}O_{3-\delta}$ at this temperature.

The XRD study of the samples after the thermal analysis gives exactly the same diffraction patterns as the initial compounds, confirming the absence of phase segregation or decomposition after the thermal treatments in air.

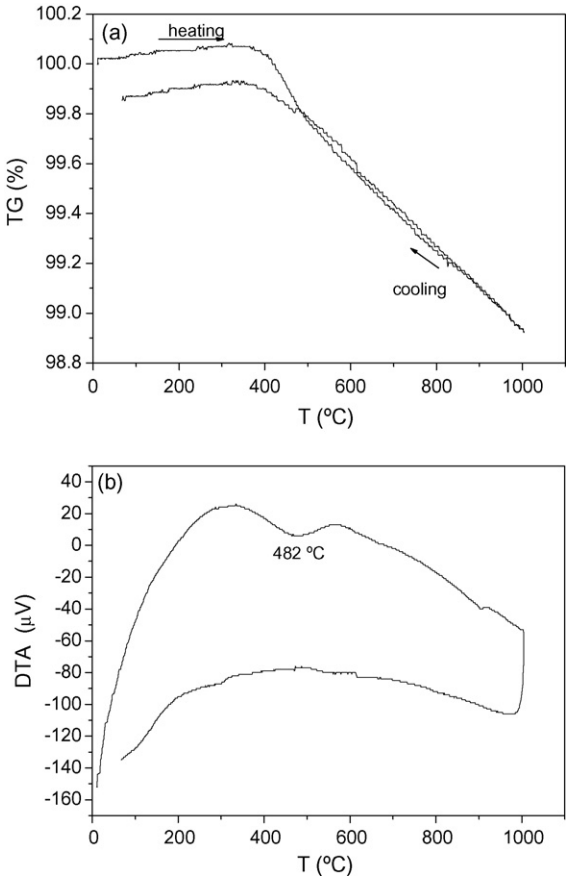

Fig. 5. Thermal analysis in air between 25 and 1000 °C for $SrCo_{0.85}Sb_{0.15}O_{3-\delta}$: (a) TG and (b) DTA.

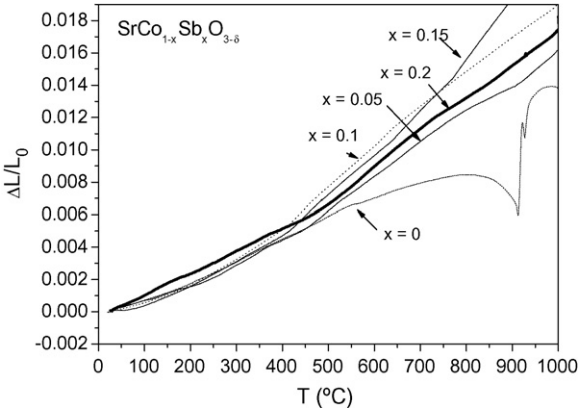

Fig. 6. Thermal expansion curves for $SrCo_{1-x}Sb_xO_{3-\delta}$.

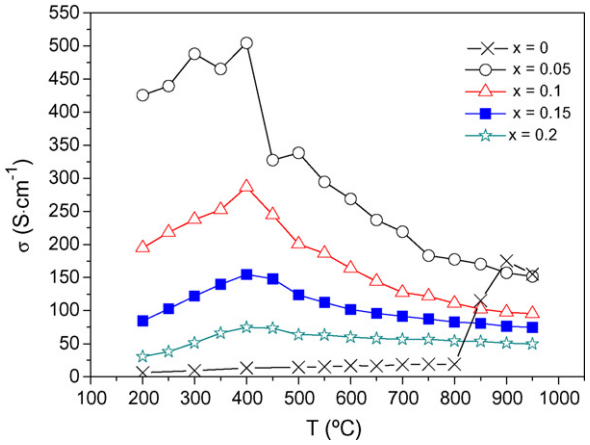

Fig. 7. Electrical conductivity as a function of temperature for $SrCo_{1-x}Sb_xO_{3-\delta}$.

3.3. Thermal expansion measurements

The thermal expansion of each compound was measured on dense cylindrical pellets sintered at 1200° C for 5 h. Fig. 6 shows a regular variation of the thermal expansion along the $SrCo_{1-x}Sb_xO_{3-\delta}$ ($0.05 \le x \le 0.2$) series without the presence of the abrupt changes observed in the undoped compound. [9]. However, the relative thermal expansion is not totally linear in all the temperature range under study. A change in the slope can be observed around 400–450 °C that could be related to the oxygen release observed by TG/DTA analysis. Moreover, for some compositions another change of slope is observed at high temperatures. Some authors [18] have related these high temperature anomalies to the reduction of Co^{3+} to Co^{2+} that could also explain the slight endothermic peak at 900 °C observed in the DTA curve (Fig. 5).

The thermal expansion coefficients obtained for the $SrCo_{1-x}Sb_xO_{3-\delta}$ system (Table 1) are considerably high for SOFC applications but they are in the range of those presented by other Co-containing perovskite like materials [19–21].

3.4. Electrical conductivity measurements

The electrical conductivity of dense pellets was obtained in air by a DC current-voltage procedure by means of the Van der Pauw four-probe method from 200 to 900 °C (Fig. 7). The undoped $SrCoO_{3-\delta}$, with hexagonal structure, shows a semiconductor-like behaviour in which the conductivity increases with temperature from 6 to 19 S cm^{-1} in the temperature range of 200–800 °C. At 800 °C the hexagonal (1D conduction) to cubic (3D conduction) phase transition takes place, leading to an overall increment of the conductivity up to 175 S cm^{-1} at 900 °C as previously reported [9].

The introduction of Sb provokes a huge increase of the electrical conductivity at temperatures ≤800 °C due to the stabilization of a 3D perovskite-like structure at RT. The highest conductivity value is presented by the $x = 0.05$ sample, reaching a maximum of 505 S cm^{-1} at 400 °C. Then, the conductivity decreases for higher temperatures obtaining 157 S cm^{-1} at 900 °C. On the other hand, there is a clear decrease in the electrical conductivity when the Sb content increases from 0.05 to 0.20, displaying a value of 51 S cm^{-1} at 900 °C for $x = 0.2$ (Fig. 7). This reduction of the electrical conductivity is due to the increment of non-conducting Sb–O bonds, which hinder the electronic transport. It is noteworthy that the electrical conductivities of pure $SrCoO_{3-\delta}$ are well below 25 S cm^{-1} in the 600–800 °C temperature range. Thus, there is an overall improvement of the electrical behaviour of the undoped hexagonal oxide after the Sb-doping in the $SrCo_{1-x}Sb_xO_{3-\delta}$ system. This enhancement is due to the stabilization of a 3D framework of corner sharing CoO_6 octahedra with open Co–O–Co angles favouring the Co(3*d*)–O(2*p*) orbital overlap and therefore the electronic conduction.

It is important to note that there is a change of the conductivity behaviour from semiconducting-like to metallic-like for temperatures higher than 400 °C for all the compositions. This transition could be related to the reduction of the sample and the lattice expansion observed at these temperatures by thermogravimetric and dilatometric analysis, respectively.

Table 1
Thermal expansion coefficients (TEC, $\times 10^{-6}$ K^{-1}) for the $SrCo_{1-x}Sb_xO_{3-\delta}$ system.

x	$TEC_{200-400\,°C}$	$TEC_{400-1000\,°C}$	$TEC_{200-1000\,°C}$
0	21.70	13.38[a]	19.34[a]
0.05	15.12	19.35	18.78
0.1	16.5	23.08	22.82
0.15	15.76	29.3	26.92
0.2	13.6	21.20	19.24

[a] For the $x = 0$ the TEC was measured till 750 °C.

3.5. Electrode performance characterization (AC impedance measurements)

The electrode performance of the system $SrCo_{1-x}Sb_xO_{3-\delta}$ was analyzed by AC impedance spectroscopy. The polarization resistance of the *x*SCSb//20CNO symmetrical cells was measured under air in OCV conditions. Fig. 8a shows the Nyquist plots obtained at 750 °C. The original impedance spectra are characterized by an ohmic contribution, mainly due to the electrolyte resistance, and the polarization contribution of the cathode/electrolyte interface. The electrolyte contribution is taken into account by the introduction of a series resistance (R_S) in the equivalent circuit employed for fitting the experimental data, whereas the polarization process is simulated by two R_P-CPE elements (R_{P1}, Q_1, R_{P2}, Q_2) (Fig. 8b). At high temperature the spectra are also affected by an inductive process coming from the experimental set up, which is taken in consideration by the introduction of a series inductance (L) in the equivalent circuit (Fig. 8b). The spectra represented in Fig. 8a have been displaced to the origin of the Z' axis after the subtraction of the series ohmic resistance in order to allow an easier comparison of the polarization process. It is clearly observed a huge decrease of the overall polarization resistance of the Sb-doped $SrCo_{1-x}Sb_xO_{3-\delta}$ ($x = 0.05$, 0.1, 0.15 and 0.2) system with a perovskite 3D-structure compared to the undoped $SrCoO_{3-\delta}$ with a hexagonal 1D-structure. The sample with the lowest Sb content, $SrCo_{0.95}Sb_{0.05}O_{3-\delta}$, displays a value of 0.038 Ω cm^2 at 750 °C, 5 times smaller than that presented by the undoped hexagonal phase. The overall electrode polarization resistance (Fig. 9) increases in parallel with the Sb content

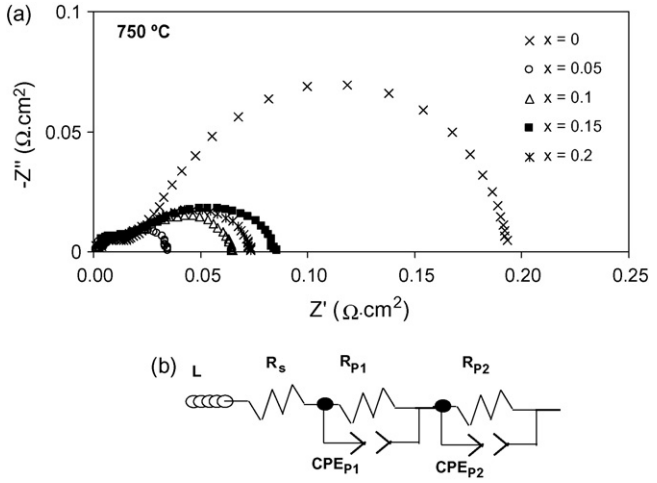

Fig. 8. (a) Nyquist plots for *x*SCSb//20CNO symmetrical cells (electrolyte resistance (R_S) was subtracted from the experimental data) and (b) equivalent circuit used for fitting the experimental data.

from $x = 0.05$ to $x = 0.15$, probably due to the reduction of oxygen vacancies content when Sb^{5+} is introduced into the structure. However, the sample with $x = 0.2$ with cubic symmetry, presents slightly lower values of electrode resistance than those of the tetragonal $x = 0.15$ perovskite. The activation energies obtained for the *x*SCSb//20CNO system are: 0.82, 0.91, 0.92 and 0.96 eV for $x = 0.05$, 0.1, 0.15 and 0.2, respectively.

It is worth noting that the polarization process in a cathode/electrolyte interface usually possesses three different contributions. The high frequency arc is usually attributed to the oxygen ion transference from the electrode-electrolyte interface to the electrolyte [22,23]. The intermediate frequency arc is usually attributed to the charge transfer reaction whereas the low frequency arc is usually attributed to the oxygen diffusion process [24]. In the system under study we have only identified the high and intermediate frequency processes which could indicate that the oxygen diffusion process is not a limiting step for the oxygen reduction and transference in the studied *x*SCSb//20CNO system.

The fitting of the experimental data to the above described equivalent circuit (Fig. 8b) allows us to analyze the effect of the Sb content on each polarization contribution. Fig. 10a shows that the polarization resistance of the high frequency arc (R_{P1}) is not highly influenced by the cathode composition. This result is in agreement with previous studies revealing that the polarization resistance associated with the oxygen ion transference from cathode/electrolyte interface to the electrolyte is mainly dependent on the electrolyte conduction process [25–27]. However, Fig. 10b evidences that the intermediate frequency arc (R_{P2}), which is attributed to the charge transfer reaction, is highly affected by the Sb-content in the $SrCo_{1-x}Sb_xO_{3-\delta}$ electrodes. The increase in the intermediate frequency resistance with the Sb-doping from $x = 0.05$ to $x = 0.15$, might be probably due to the decrease of the oxygen vacancies content of the $SrCo_{1-x}Sb_xO_{3-\delta}$ system hindering the charge transfer reaction. The results obtained in Figs. 9 and 10 suggest that the charge transfer reaction is the limiting step in the overall electrode polarization. Note that the improvement in the electrode performance obtained for $x = 0.2$ compared to $x = 0.15$ could be due to the cubic phase transition obtained for $x = 0.2$.

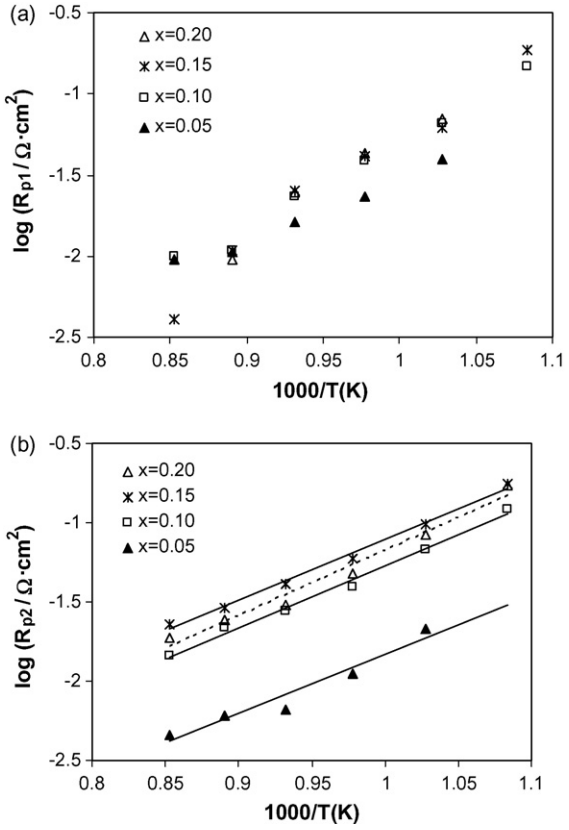

Fig. 10. (a) Electrode polarization contribution due to (a) process 1 (R_{P1}) and (b) process 2 (R_{P2}) as a function of Sb content at the *x*SCSb//20CNO symmetrical cells.

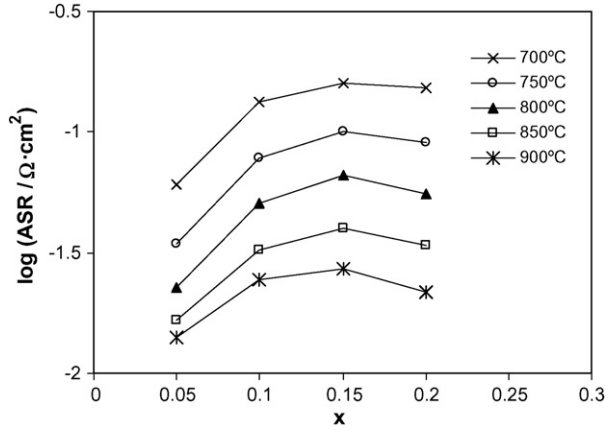

Fig. 9. Area specific resistance at different temperatures for the *x*SCSb//20CNO system.

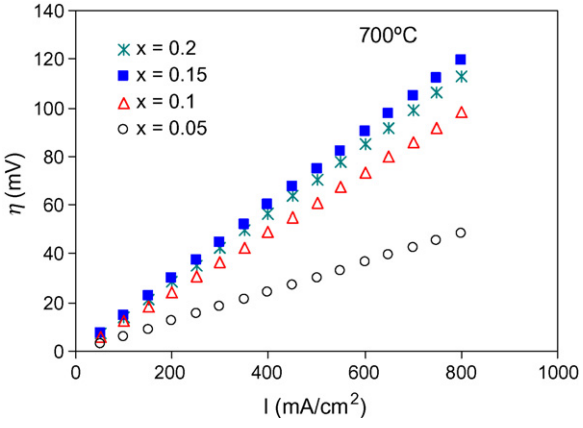

Fig. 11. Cathodic overpotential for *x*SCSb//20CNO as a function of the current flux.

Fig. 11 shows the cathodic overpotential at 700 °C for the $SrCo_{1-x}Sb_xO_{3-\delta}$ system working with 20CNO electrolyte as a function of the current flux. It is worth noting the low overpotential obtained for $x = 0.05$, which is sensibly increased for higher contents of Sb. The results reveal values from 40 to 120 mV for a current value of 800 mA cm^{-2}, which indicates the very good performance of $SrCo_{1-x}Sb_xO_{3-\delta}$ cathode system working with 20CNO electrolyte. On the other hand, if the internal resistances of the cell (anode and cathode polarization and electrolyte resistance) are not current dependent, we can assume that the theoretical maximum power density is only dependent on the open circuit voltage (OCV), for the used electrolyte, and the internal resistances of the cell [25]. The low polarization resistances obtained along the $SrCo_{1-x}Sb_xO_{3-\delta}$ series compared with other cathodes with ceria-based electrolytes [28,29] suggest the possibility of obtaining high power densities in SOFC for these materials in ceria-based systems. The good performance of $SrCo_{0.95}Sb_{0.05}O_{3-\delta}$ was confirmed by the estimation of a value of maximum power density higher than 300 mW cm^{-2} at 700 °C assuming an electrolyte thickness of 200 μm in a ceria-based SOFC. For this purpose we have introduced the typical values of 0.85 V and 0.1 Ω cm^2 for the OCV and the anode polarization, respectively, previously obtained for ceria-based systems [28]. This stands out the $SrCo_{0.95}Sb_{0.05}O_{3-\delta}$ as an excellent candidate to be used as cathode material in temperature solid oxide fuel cells.

4. Conclusions

In order to stabilize a 3D perovskite-like structure with low doping levels, the oxides $SrCo_{1-x}Sb_xO_{3-\delta}$ ($x = 0.05$, 0.1, 0.15 and 0.2) have been synthesized as new materials by the citrate-nitrate route. The introduction of Sb in the undoped hexagonal $SrCoO_{3-\delta}$ allows the stabilization of a tetragonal 3D perovskite structure for doping levels between 0.05 and 0.15, whereas for $x = 0.2$ a cubic *Pm-3m* perovskite is obtained. The Sb-doping also produces an enhancement of the thermal stability avoiding the presence of reconstructive structural transitions and eliminating abrupt changes in the thermal expansion. Moreover, there is also a great increment of the electrical conductivity at intermediate and low temperatures ($T \leq 800$ °C) compared to the undoped $SrCoO_{3-\delta}$. The electrical conductivity increases with the decrease in the Sb-content, obtaining a value as high as 500 S cm^{-1} at 400 °C and above 160 S cm^{-1} in the usual range of SOFC working conditions (650–900 °C) for the sample $x = 0.05$. The polarization resistance of the cathode-electrolyte interface is greatly decreased with the Sb introduction when the system is working with $Ce_{0.8}Nd_{0.2}O_{2-\delta}$ as electrolyte, and all the samples display values below 0.1 Ω cm^2 for $T \geq 750$ °C. However the performance is higher for lower contents of Sb, and the sample with $x = 0.05$ possesses values of polarization resistance between 0.009 and 0.23 Ω cm^2 from 900 to 600 °C and estimated values of power density higher than 300 mW cm^{-2} at 700 °C in ceria-based SOFC. These results allow us to propose this material as an excellent candidate to be used as cathode component in intermediate solid oxide fuel cell.

Acknowledgements

This work was sponsored by Community of Madrid (ENERCAM, Ref-S-0505/ENE-304) and Innovation and Science Ministry (MAT-SOFC, Ref-MAT2005-02933 and MAT2007-60536). Ministerio de Innovación y Ciencia is grateful to the Innovation and Science Ministry for financial support ("Programa Juan de la Cierva").

References

[1] Z.Q. Deng, W.S. Yang, W. Liu, C.S. Chen, J. Solid State Chem. 179 (2006) 362.
[2] L.W. Tai, M.M. Nasrallah, H.U. Anderson, D.M. Sparlin, S.R. Sehlin, Solid State Ionics 76 (1995) 259.
[3] W.C. Hansen, L.T. Brownmiller, R.H. Bogue, J. Am. Chem. Soc. 50 (1928) 396.
[4] J.G. Grenier, S. Ghodbane, G. Demazeau, M. Pouchard, P. Hagenmuller, Mater. Res. Bull. 14 (1979) 831.
[5] P.D. Battle, T.C. Gibb, A.T. Steel, J. Chem. Soc., Dalton Trans. (1987) 2359.
[6] P.D. Battle, T.C. Gibb, J. Chem. Soc., Dalton Trans. (1987) 667.
[7] P.D. Battle, T.C. Gibb, A.T. Steel, J. Chem. Soc., Dalton Trans. (1988) 83.
[8] W. Harrison, S.L. Hedwood, A.J. Jacobson, J. Chem. Soc., Chem. Commun. (1995) 1953.
[9] C. de la Calle, A. Aguadero, J.A. Alonso, M.T. Fernandez-Diaz, Solid State Sci. 10 (2008) 1924.
[10] T. Nagai, W. Ito, T.R. Sakon, Solid State Ionics 177 (2007) 3433.
[11] Z.Q. Deng, W. Liu, C.S. Chen, H. Lu, W.S. Yang, Solid State Ionics 170 (2004) 187.
[12] P. Zeng, R. Ran, Z. Chen, W. Zhou, H. Gu, Z. Shao, S. Liu, J. Alloys Compd. 455 (2008) 465.
[13] Y. Teraoka, H.-M. Zhang, S. Furukawa, N. Yamazoe, Chem. Lett. (1985) 1743.
[14] K. Wiik, S. Aasland, H.L. Hansen, I.L. Tangen, R. Odegard, Solid State Ionics 152–153 (2002) 675.
[15] A. Aguadero, C. de la Calle, J.A. Alonso, M.J. Escudero, M.T. Fernandez-Díaz, L. Daza, Chem. Mater. 19 (2007) 6437.
[16] D. Pérez-Coll, P. Núñez, J.R. Frade, J.C.C. Abrantes, Electrochim. Acta 48 (2003) 1551.
[17] J.C.C. Abrantes, D. Pérez-Coll, P. Núñez, J.R. Frade, Electrochim. Acta 48 (2003) 2761.
[18] B. Wei, Z. Lu, X. Huang, J. Miao, X. Sha, X. Xin, W. Su, J. Eur. Ceram. Soc. 26 (2006) 2827.
[19] N. Orlovskaya, M. Lugovy, S. Pathak, D. Steinmetz, J. lloyd, L. Fegeley, M. Radovic, E.A. Payzant, E. Lara-Curzio, L.F. Allard, J. Kuebler, J. Power Sources 182 (2008) 230.
[20] Q. Zhu, T. Jin, Y. Wang, Solid State Ionics 177 (2006) 1199.
[21] H.L. Lein, K. Wiik, T. Grande, Solid State Ionics 177 (2006) 1795.
[22] C. Fu, K. Sun, N. Zhang, X. Chen, D. Zhou, Electrochim. Acta 52 (2007) 4589.
[23] M.J. Escudero, A. Aguadero, J.A. Alonso, L. Daza, J. Electroanal. Chem. 611 (2007) 107.
[24] X. Xu, Z. Jiang, X. Fan, C. Xia, Solid State Ionics 177 (2006) 2113.
[25] D. Perez-Coll, A. Aguadero, M.J. Escudero, P. Nuñez, L. Daza, J. Power Sources 178 (2008) 151.
[26] E.P. Murray, S.A. Barnett, Solid State Ionics 143 (2001) 265.
[27] E.P. Murray, T. Tsai, S.A. Barnett, Solid State Ionics 110 (1998) 235.
[28] X. Fang, G. Zhu, C. Xia, X. Liu, G. Meng, Solid State Ionics 168 (2004) 31.
[29] S. Wang, T. Kato, S. Nagata, T. Kaneko, N. Iwashita, T. Honda, M. Dokiya, Solid State Ionics 152–153 (2002) 477.